Rapid 21st century weakening of the Agulhas Current in a warming climate

Ruize Zhang[1,2,3], Shantong Sun[*4], Zhaohui Chen[*1,2], Haiyuan Yang[1,2] and Lixin Wu[1,2]

1. Frontier Science Center for Deep Ocean Multispheres and Earth System (FDOMES) and Physical Oceanography Laboratory, Ocean University of China, Qingdao, China
2. Laoshan Laboratory, Qingdao, China
3. Academy of the Future Ocean, Ocean University of China, Qingdao, China
4. Department of Earth, Ocean & Atmospheric Science, Florida State University, Tallahassee, US

[*] *Corresponding author*:

Shantong Sun (ssun5@fsu.edu)

Zhaohui Chen (chenzhaohui@ouc.edu.cn)

Key Points:

- Climate models consistently project the Agulhas Current to weaken in the 21st century
- Changes in Indo-Pacific wind and Atlantic overturning both contribute to the projected Agulhas Current weakening
- The Agulhas Current becomes shallower in a warming climate mainly due to the weakening of the Atlantic overturning

Abstract

The Agulhas Current (AC) is a critical component of the global ocean circulation. Climate models consistently project the AC to decline in the 21st century. Previous studies typically attributed the weakening of AC to changes in Indian Ocean wind and a decline of the Indonesian Throughflow (ITF) transport. However, our analysis suggests that changes in local surface wind and ITF can only explain a portion of the model-simulated AC changes. Using a hierarchy of models, we show that the decline of the Atlantic Meridional Overturning Circulation (AMOC) strength in a warming climate could also contribute substantially to the AC weakening. Following a weakening of the AMOC, the baroclinic structure of the AC is modified such that the AC is shoaled to a shallower depth, communicated between basins via Kelvin waves. Our results highlight the importance of remote processes in future western boundary current changes.

Plain Language Summary

The Agulhas Current (AC) is one of the strongest currents in the ocean and plays an important role in the climate system. Climate models consistently project a rapid weakening of the AC during the 21st century. Traditionally, the weakening of the AC has been attributed to changes in local surface wind and the Indonesian Throughflow (ITF), which transports water from the Pacific Ocean to the Indian Ocean. However, our analysis suggests these changes cannot fully explain the AC changes in a warming climate. In this study, we show that remote processes in the North Atlantic could also contribute substantially to the AC weakening. In a warming climate, the Atlantic overturning circulation slows down and modifies the density structure of the Atlantic, which propagates into the Indian Ocean via wave processes and causes a weakening and shoaling of the AC. Our results highlight the importance of remote processes in future ocean circulation changes.

1. Introduction

The Agulhas Current (AC) is the strongest western boundary current in the Southern Hemisphere and plays a critical role in the climate system (Beal et al., 2011). Originating from the Mozambique Channel and the Southeast Madagascar Current, the AC transports around 76 Sv of warm water poleward (Beal et al., 2015; McMonigal et al., 2020). After passing the southern tip of Africa, the AC retroflects back into the Indian Ocean, with a significant amount of warm and salty water leaked into the Atlantic, acting as a warm route for the surface returning branch of the Atlantic Meridional Overturning Circulation (AMOC; Biastoch et al., 2008b; Rühs et al., 2013; Wang et al., 2016). Thus, the AC plays a crucial role in connecting major ocean basins and could potentially modulate the variability of the global ocean overturning circulation (Weijer et al., 2002; Biastoch et al., 2008a; Talley, 2013). In this study, we focus on the centennial responses of the AC volume transport to the increasing greenhouse gas forcing. Climate models consistently project the AC volume transport to decline in the 21st century (Stellema et al., 2019; Sen Gupta et al., 2021). Here we argue that remote processes in the North Atlantic are as important as local processes (e.g., surface wind) in determining the AC changes in a warming climate.

The global ocean circulation is expected to change in a warming climate, but not uniformly (Chen et al., 2019; Hu et al., 2020; Peng et al., 2022). In response to the increasing greenhouse gas forcing, the atmospheric circulation evolves with a poleward shift in the westerly wind in both hemispheres (Chen et al., 2008; Goyal et al., 2021). This shift in the westerly wind leads to a poleward expansion of the subtropical gyre circulation (Yang et al., 2020) and could potentially contribute to a weakening of the western boundary currents (Ma et al., 2020). This wind changes have been suggested to contribute to the weakening of AC in a warming climate (Stellema et al., 2019). On the other hand, as the climate warms, sea surface temperature increases and leads to a stronger upper-ocean density stratification (Capotondi et al., 2012; Li et al., 2020). The stronger density stratification limits the vertical momentum input into the subsurface ocean, causing a spin-up of the upper ocean circulation and a spin-down of the subsurface ocean circulation (Sun et al., 2013; Chen et al., 2019; Peng et al., 2022; Zhang et al., 2017). This stratification change has been invoked in explaining the strengthening of the Kuroshio Current (Chen et al., 2019).

Previous studies on the long-term weakening of the AC transport have primarily focused on changes in the local surface wind forcing and the Indonesian Throughflow (ITF) (Stellema et al.,

2019; Ma et al., 2020). In the mean state, the upper-ocean volume transports across the boundaries of a basin are balanced and, thus, the AC volume transport can be expressed as a combination of the ITF volume transport and the wind-driven Sverdrup transport across the Indian Ocean (green arrows in Figure 1), i.e.,

$$V_{\mathrm{AC}} = V_{\mathrm{ITF}} + \int_{x_{\mathrm{w}}}^{x_{\mathrm{e}}} \frac{\mathrm{curl}\ \vec{\tau}}{\beta \rho_0} dx, \qquad (1)$$

where V_{AC} and V_{ITF} represent the volume transport of the AC (positive for southward transport) and ITF (positive for transport into the Indian Ocean), respectively, curl$\vec{\tau}$ is the curl of surface wind stress, β is the meridional gradient of the Coriolis parameter, ρ_0 is the reference seawater density. Critically, the interior diapycnal upwelling in the Indian Ocean might also contribute to the volume transport of AC, but it is small, ~1 Sv, compared to the upper-ocean transport (Text S1). In a warming climate, the ITF volume transport is projected to decline (Sen Gupta et al., 2016; Feng et al., 2017) and the Indian Ocean wind stress curl is expected to develop a negative anomaly at around 30˚S, as the Southern Hemisphere westerly wind shifts southward both contributing to a weaker AC (purple arrows in Figure 1). However, as we estimated in Section 2, changes in the ITF and Indian Ocean wind stress forcing explain less than 60% of the AC volume transport decrease in most of the climate models examined in this study. This discrepancy arises because the upper-ocean volume transport balance in Eq. (1) is not satisfied in transient responses due to a volume transport convergence that exists in balance with the deepening of isopycnal surfaces, following a weakening of the AMOC (Sun et al., 2020; Sun et al., 2022).

Due to surface warming and freshening in the high-latitude North Atlantic, the AMOC is expected to slow down in the 21st century with a reduced formation of North Atlantic Deep Water (NADW; Cheng et al., 2013; Weijer et al., 2020). The reduction in NADW formation causes a deepening of isopycnals in the high-latitude North Atlantic. The isopycnal deepening signal propagates into the South Atlantic and Indian Ocean via Kelvin waves and Rossby waves (Huang et al., 2000), leading to geostrophically-balanced, volume transport anomalies that are opposite between the Atlantic and Indo-Pacific basins (Sun et al., 2020; Sun and Thompson, 2020). Building on this idea, we show that the isopycnal deepening along the western boundary of the Indian Ocean could modify the baroclinic structure of the AC and contribute substantially to the projected AC weakening in the 21st century.

147 Our main approach is to use a hierarchy of ocean and climate models to investigate the
148 physical processes responsible for the projected rapid weakening of the AC in a warming climate.
149 We first use a suite of coupled climate model simulations to estimate how much of the AC
150 weakening in a warming climate can be explained by changes in local surface wind and ITF, as
151 described in Section 2. We then use a reduced gravity model and an ocean-only general
152 circulation model to illustrate the key processes for the AMOC to influence the AC volume
153 transport in Sections 3 and 4. We summarize the main results in Section 5.
154

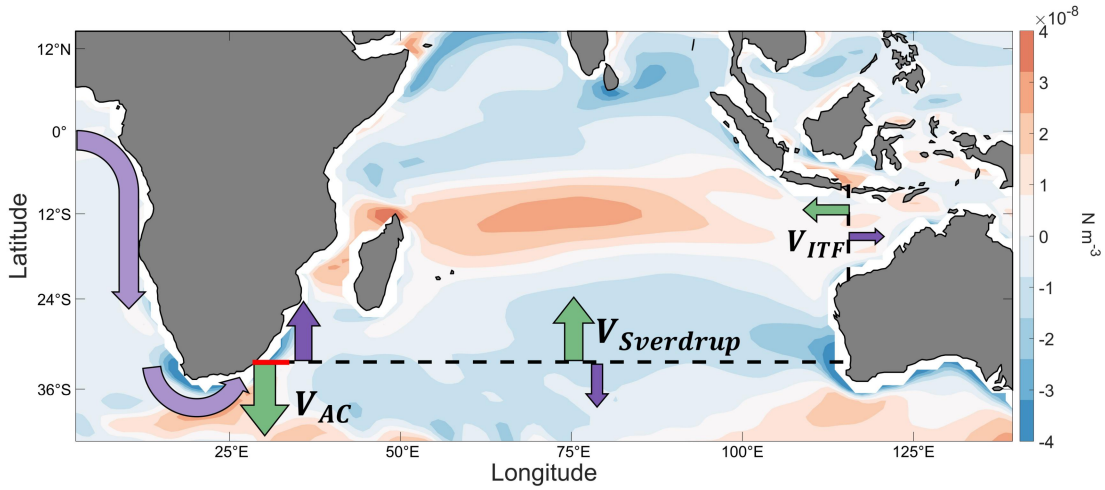

155

156 **Figure 1.** A schematic of the Indian Ocean circulation and its changes. The background color
157 represents changes in wind stress curl from 2006 to 2100 in CESM Large Ensemble. The red line
158 denotes the cross-section for evaluating the AC volume transport. The green arrows represent the
159 direction of time-mean circulation and the purple arrows represent the changes. The light purple
160 arrows around the African continent indicate the pathway by which the AMOC affect the AC.
161

162 **2. Agulhas Current changes in climate models**

163 To evaluate how much of the AC changes in a warming climate can be explained by local
164 *vs* remote processes, we use model output from the Community Earth System Model Large
165 Ensemble (CESM-LENS) (Kay et al., 2015) under a high-emission scenario of Representative
166 Concentration Pathway 8.5 (RCP8.5) from 2006 to 2100. We calculate the ensemble mean of the
167 40 CESM-LENS members. The AC volume transport across 32.5˚S (red line in Figure 1),
168 integrated from the sea surface to 2000 m depth and averaged between 2006 and 2015, is 69.2 Sv,
169 which is close to observations (Beal et al., 2015; Bryden et al., 2005; Gunn et al., 2020;

McMonigal et al., 2020). From 2006-2100, the AC volume transport declines substantially by about 16.5 Sv (Figure 2a), or ~24%.

Changes in the Indian Ocean surface wind and ITF cannot fully explain the projected AC transport decrease (cf., Ma et al., 2020). The negative wind stress curl anomaly in the Indian subtropics corresponds to a weakening of the interior Sverdrup transport and thus a decline of the southward volume transport by the AC [Eq. (1) and Figure 1]. At 32.5˚S, we estimate that this change contributes 4.4 Sv to the AC volume transport reduction from 2006 to 2100 (Figure 2b). The ITF volume transport declines by about 4.2 Sv from 2006 to 2100 (Figure 2b). Taken together, changes in the Indian Ocean surface wind and ITF volume transport explain 52% of the AC weakening (pink line vs blue line in Figure 2a). Critically, part of the ITF volume transport reduction may be driven by remote changes in the North Atlantic (Sun and Thompson, 2020). We estimate the ITF volume transport reduction due to changes in local Indo-Pacific surface wind based on the Island Rule constraint and conclude that local processes only account for 1.6 Sv of the ITF reduction (Figure S1, Godfrey, 1989), with the remaining 2.6 Sv related to the weakening of the AMOC (Sun and Thompson 2020). We note that the Island Rule calculation is sensitive to the choice of integral pathway, but the conclusion should be robust qualitatively.

Similar conclusions are drawn for models that participate the Coupled Model Intercomparison Project, phase 6 (CMIP6) (Eyring et al., 2016). We examined the circulation changes in 20 CMIP6 climate models under the high-end emission scenario ("SSP585") from 2015 to 2100. As the climate warms, all 20 models exhibit a declining trend in the AC volume transport, ranging from 10 Sv to 35 Sv. In 12 models, changes in the Indian Ocean wind and ITF transport explain less than 60% of the AC weakening (Figure S2). Only in five of the 20 models, changes in the Indian Ocean wind and ITF transport explain more than 80% of the AC weakening. A brief discussion on the inter-model spread is included in Section 5. Nonetheless, these results suggest that there is another process in play that influence the transient responses of the AC volume transport. Here we argue it is the weakening of the AMOC that accounts for the discrepancies between the simulated AC volume transport changes and previous expectations based on the mean-state upper-ocean volume transport balance (Eq. 1). In the next section, we illustrate the processes by which the AMOC weakening could contribute to the AC volume transport decrease using a 1.5-layer reduced gravity model.

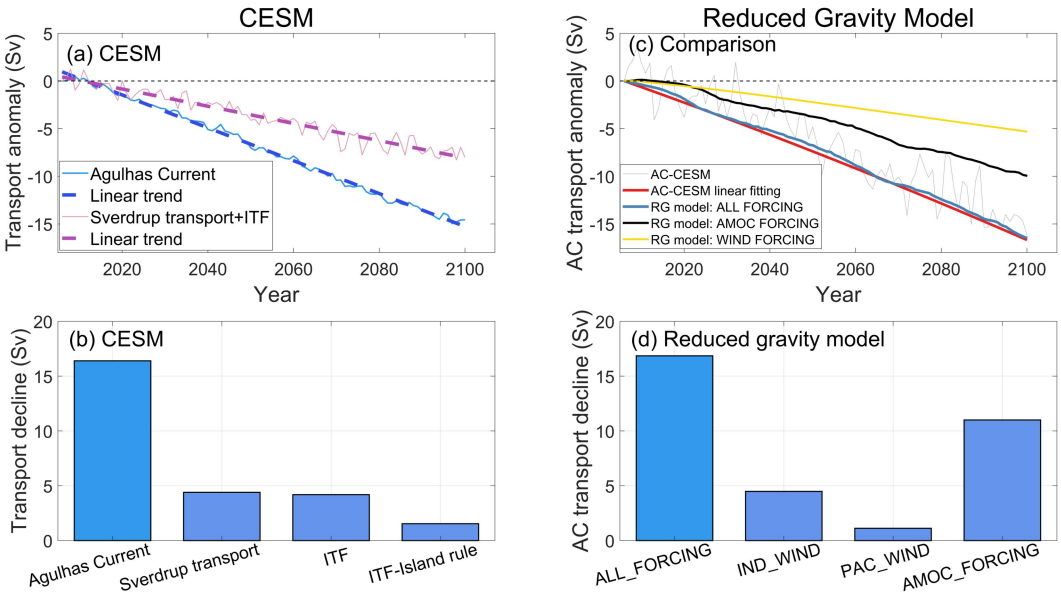

Figure 2. Comparison of different processes in contributing to the AC volume transport reduction in CESM and the reduced gravity model. (a) Evolution of the ensemble- and annual-mean AC volume transport anomaly (blue solid line) and its linear trend (blue dashed line) in CESM-LENS during 2006-2100. The sum of the annual-mean Sverdrup transport anomaly and ITF volume transport anomaly (purple solid line) as well as its linear trend (purple dashed line) during 2006-2100 are plotted for comparison. (b) The decline of the AC volume transport from 2006 to 2100 in CESM and the contributions due to changes in Sverdrup transport and ITF volume transport. The ITF volume transport reduction due to Indo-Pacific wind changes is estimated based on the Island Rule constraints. (c) The AC volume transport anomaly (Sv) simulated by the reduced gravity model (blue line) as compared to the CESM-LENS member (gray line) and its linear fitting (red line). The AC volume transport anomaly forced by the AMOC alone and the Indo-Pacific wind alone is plotted as a black and yellow line. (d) The decline of the AC volume transport (Sv) simulated by the reduced gravity model from 2006 to 2100. Changes in (b) and (d) are calculated as the linear trend during 2006-2100, multiplied by 94 years.

3. Agulhas Current changes in a reduced gravity model

In this section, we use a 1.5-layer reduced gravity model to investigate the role of AMOC weakening and Indo-Pacific wind changes in driving the decline of the AC volume transport, projected for the 21st century. Reduced gravity models have proven in previous studies to be useful tools in guiding theoretical discussions of the physical processes that govern the large-scale circulation (Johnson and Marshall, 2004; Allison et al., 2011; Chen et al., 2014; Sun et al., 2020).

We use the 1.5-layer reduced gravity model developed in Sun and Thompson (2020). The model is an idealized representation of the wind-driven gyre circulation and the upper branch of

the global ocean overturning circulation. The model domain includes three idealized ocean basins representative of the Atlantic, Indian, and Pacific, connected by a zonally re-entrant channel that represents the Southern Ocean (Figure S3a). The model evolves the upper layer thickness h in the ocean. The formation of NADW is represented as a prescribed downwelling velocity in the high-latitude North Atlantic. Surface water mass transformation in the Southern Ocean is represented as a relaxation of the upper layer thickness to 10 m close to the southern boundary. The relaxation timescale increases from 10 days at the southern boundary to 100 days at 62 ˚S. As such, the Southern Ocean overturning circulation is allowed to evolve as the global-mean interface depth changes in the northern basins. Interior diapycnal mixing is parameterized as a diapycnal upwelling velocity, $w_{diap} = \kappa/h$, with $\kappa = 2.0 \times 10^{-5}$ m^2 s^{-1}. The interior diapyancal mixing contributes about 1 Sv of diapycnal upwelling, close to that in CESM-LENS (Text S1). The unresolved mesoscale eddies are parameterized as a thickness diffusion with the diffusivity K_{GM} = 1000 m^{2}s^{-1} (Gent and Mcwilliams, 1990). We force the reduced gravity model with annual-mean surface wind stress and NADW formation rate derived from the first member of CESM-LENS. The NADW formation rate in CESM is calculated as the maximum value of the AMOC streamfunction at 40 ˚N and is prescribed in the reduced gravity model as a downward velocity close to the northern boundary of the Atlantic basin. A detailed description of the model configuration is provided in Text S2 of the supporting information. As a control, we integrate the reduced gravity model, forced by the annual-mean surface wind stress (Figure S3a) and NADW formation rate from CESM at year 2006, for 4000 years to reach an approximately steady state. Using control as initial conditions, we conduct another four simulations, summarized in Table 1, to quantify the contributions to the weakening of the AC due to changes in the Indo-Pacific wind and AMOC (Figure S4).

TABLE 1. Description of the reduced gravity model experiments. “CESM” means the forcing evolves as in CESM during 2006-2100; “Control” means the forcing is fixed at year 2006 as in the control run.

EXPERIMENTS	INDIAN WIND	PACIFIC WIND	AMOC FORCING
IND_WIND	CESM	Control	Control
PAC_WIND	Control	CESM	Control
AMOC_FORCING	Control	Control	CESM
ALLFORCING	CESM	CESM	CESM

When forced with both the Indo-Pacific wind and NADW formation rate that evolve as in CESM during 2006-2100 ("ALLFORCING"), the reduced gravity model approximately reproduces the AC volume transport changes (compare the blue and red lines in Figure 2c). This suggests that the reduced gravity model captures the key dynamics in driving the projected AC weakening in CESM. When we only evolve the Indian Ocean wind as in CESM and fix the Pacific wind and the AMOC as in Control ("IND_WIND"), the reduced gravity model only simulates a weakening of the AC by 4.4 Sv (Figure 2d), consistent with the estimated Sverdrup transport changes in CESM (Figure 2b). When we only evolve the Pacific surface wind as in CESM during 2006-2100 ("PAC_WIND"), the reduced gravity model simulates a weakening of the AC by 1.1 Sv. This number is much smaller than the decline of ITF volume transport (~4.2 Sv) in CESM, but it is close to our estimate from changes in the Indo-Pacific wind based on the Island Rule constraints (1.6 Sv in Figure 2b). The discrepancy arises because much of the projected ITF changes in CESM are driven by the weakening of the AMOC (Sun and Thompson, 2020), which is not represented in "PAC_WIND". To identify the impacts from the weakening of the AMOC, we carry out "AMOC_FORCING", in which we fix the surface wind stress and only evolve the NADW formation rate as in CESM. The weakening of the AMOC leads to a decline of the AC volume transport by about 11 Sv (Figure 2c & d). Taken together, changes in the Indo-Pacific wind and AMOC explains the decline of the AC volume transport. The impact of AMOC exceeds the contributions due to surface wind changes, highlighting the role of remote processes in the projected decline of the AC volume transport.

The remote North Atlantic processes influence the AC volume transport via wave propagations. As the AMOC slows down in a warming climate, the isopycnals in the high latitude North Atlantic becomes deeper (Sun et al., 2020). The deepening signal propagates as Kelvin waves along the coast and the equator to the western boundary of the Indian Ocean (Figure S5; Huang et al., 2000). The isopycnal deepening on the western boundary corresponds to a northward geostrophic transport anomaly, i.e., a slow-down of the AC (Figure S6 for the reduced gravity model).

Despite the idealized nature of the reduced gravity model, the physical processes linking changes in the AMOC to the AC discussed above appears to be also relevant in more realistic simulations (Figures 2 & 3). In CESM, there is a positive anomaly in the offshore density

gradient across the AC, most pronounced at 1-2 km depths, consistent with a deepening of isopycnals along the western boundary (Figure 3b & S7). This depth range aligns well with the structure of the AMOC weakening in CESM, which also peaks at 1-2 km (Figure 3a). The density anomaly corresponds to a slow-down of the AC through geostrophy.

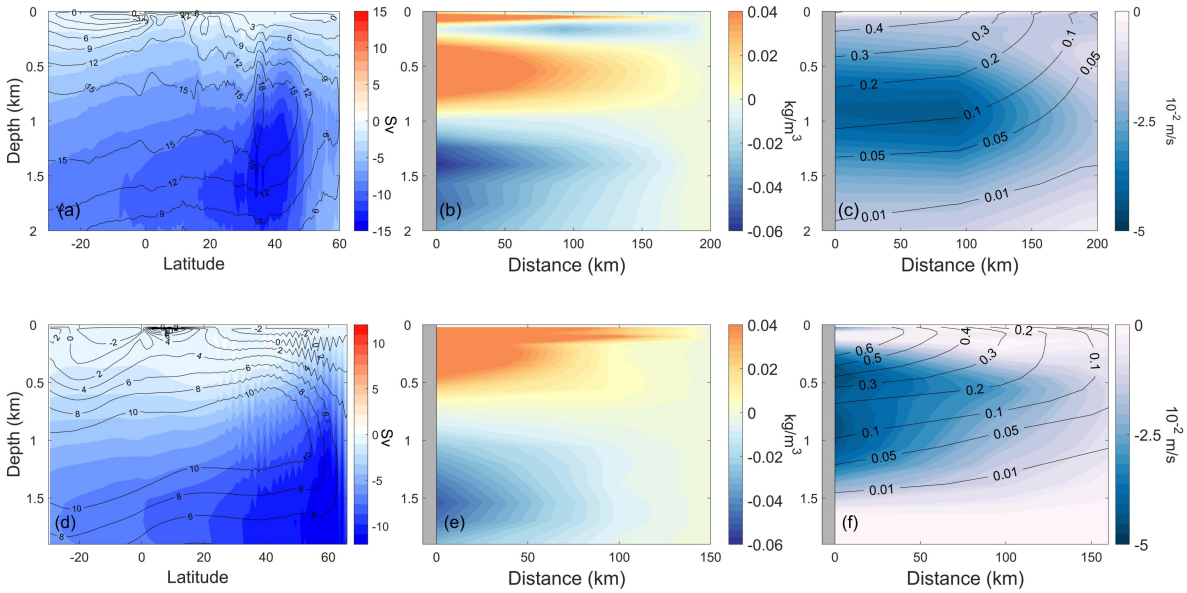

Figure 3. Connecting the shoaling of the AC to AMOC weakening. (a) Changes in the AMOC streamfunction from 2006 to 2100 in the CESM-LENS (background color), calculated as 94 times the linear trend. The black contours denote the time-mean AMOC streamfunction averaged between 2006 and 2100 (positive for clockwise overturning). (b) Changes in in-situ density (kg/m^3) along the AC cross-section (red line in Figure1) from 2006 to 2100 in CESM-LENS. The density anomaly on the right boundary (x=200 km) is subtracted to highlight the offshore density gradient. The gray patch in the left side denotes the coast of Africa. (c) Velocity changes (m/s) in the AC section from 2006 to 2100 in CESM-LENS (negative for AC slowdown). The black contours denote the time-mean velocity of AC averaged between 2006 and 2100. The gray patch in the left side denotes the coast of Africa. (d, e, f) Same as above but for the "AMOC weakening" experiment carried out with MITgcm. The anomalies are calculated as the difference between the "AMOC weakening" run and control run, averaged over the last 20 years.

4. Shoaling of the AC in a warming climate

The weakening of the AC is accompanied by a change in its depth structure. In CESM-LENS, the velocity field of the AC throughout the upper 2 km exhibits a decreasing trend, which peaks at about 1 km depth (Figure 3c) and represents a shoaling of the AC depth. Defined as the maximum depth of the 1 cm/s velocity contour, the depth of AC is shoaled from 1700 m at 2006

to 1300 m at 2100 (Figure S8). Similar shoaling of the AC is present in other climate models that participate CMIP6 (Figure S9 & S10). Both the AMOC weakening and the stronger surface stratification in a warming climate may contribute to this shoaling of the AC (e.g., Peng et al., 2022). Here we use a suite of ocean-only simulations to show that this shoaling of the AC is mainly driven by the remote AMOC changes.

We use the Massachusetts Institute of Technology General Circulation Model (MITgcm; Marshall et al., 1997) to carry out the ocean-only simulations. The model uses the same geometry as the reduced gravity model. The model domain has 30 vertical layers ranging from 20 m at the top to 250 m at the bottom. There is only one thermodynamic variable, temperature, for simplicity. We perturb the AMOC through a warming in the high-latitude North Atlantic. A detailed discussion of the model setup is provided in Text S3 of the supporting information. As a control run, we run the model for 2000 years to reach an approximately steady state. Using the control run as initial conditions, we evaluate the role of remote and local processes in driving the AC changes. Two experiments are designed: "AMOC weakening" and "Indian Ocean warming".

In "AMOC weakening", we apply a 3 ˚C sea surface warming in the high-latitude North Atlantic from 71.5 ˚N to 67.5 ˚N. This surface warming strengthens the upper-ocean stratifications in the North Atlantic and leads to a decline of the AMOC strength by 6 Sv (Figure 3d & S12). Similar to CESM, there is also a positive anomaly in the offshore density gradient across the AC. This density gradient anomaly is most pronounced at 1-2 km depths and corresponds to a deepening of the isopycnal driven by an AMOC weakening (Figure 3d, e). The AMOC weakening causes the AC volume transport to decrease by a similar magnitude of around 6 Sv (Figure S12), largely consistent with the reduced gravity model in Section 3. The velocity field shows a decreasing trend through the upper 1.6 km. The decreasing trend peaks at around 0.8 km depth, slightly shallower than CESM, which is not unexpected considering their different model configurations. The depth of AC, defined as the maximum depth of 1 cm/s velocity contour, shoals by about 200 m in the "AMOC weakening" (Figure S11).

The surface warming in the Indian Ocean could also contribute to the subsurface weakening of the AC (Peng et al., 2022). Here we test this idea by applying a 3˚C warming in the Indian Ocean ("Indian Ocean warming" run). Consistent with previous studies, the surface warming leads to a spin-up of the upper ocean circulation and a spin-down of the subsurface gyre circulation (Figure S13). However, these changes are confined to the upper 600 m and does not

appear to affect the AC depth by our definition (Figure S11). When integrated vertically, the surface spin-up and subsurface spin-down also cancels out, leading to minimal changes in the AC volume transport (Figure S12).

We also examined the influence of the Southern Hemisphere (SH) westerly wind in the AC changes. The SH westerly wind is projected to strengthen in a warming climate (Goyal et al., 2021) and may also contribute to the AC changes. However, our results suggest that a strengthening of the SH westerly wind by 10%, comparable to the projected changes in CMIP6, could only slightly weaken the AC in the upper 300 m, but strengthen the AC from 300 m to 800 m depth (Figure S14).

5. Summary and Discussions

Climate models consistently project a weakening of the Agulhas Current (AC) during the 21st century. Previous studies typically attributed this weakening to changes in the local surface wind stress or/and ITF volume transport. However, our analysis suggests these changes cannot fully explain the AC changes in climate model simulations. Here we revisit the physical processes in driving the AC weakening and highlight the role of AMOC weakening as an additional process in contributing to the AC changes. In response to the increasing greenhouse gas forcing, the AMOC slows down and modifies the baroclinic structure of the AC, communicated between basins by waves. This process leads to a weakening and shoaling of AC in a warming climate during the 21st century.

The 21st century projections for the AC transport stand in contrast with the historical changes. During the historical period, it remains debatable whether the AC strength has changed significantly in response to greenhouse gas forcing (cf. Beal and Ellipot, 2016). Recently, using a hierarchy of ocean and climate models, Zhang et al. (2023) showed that the AC is characterized by substantial decadal and multi-decadal variabilities, which complicated the interpretation of the AC responses based on a short observational period during the historical period.

Although the dynamical connection between the AMOC and the Agulhas Current is robust, our results suggest significant inter-model spread in how much the AMOC explains the projected Agulhas Current changes in the 21st century (e.g., Figure S2). This may arise from the inter-model spread in the projected AMOC weakening during the 21st century (e.g., Bonan et al., 2022;

Bellomo et al., 2021) or the inter-model spread in the projected wind changes (e.g., Sen Gupta, 2016).

We emphasize that the remote impact of AMOC weakening on the Agulhas Current is a transient process that is mostly highlighted on decadal to centennial timescales. On longer timescales, as the isopycnal deepens in the Indo-Pacific basin, the Southern Ocean overturning circulation will gradually play a bigger role in balancing the AMOC changes on multi-centennial timescales (Sun et al., 2020). Eventually, the Agulhas Current will be in balance with the local Sverdrup transport and ITF volume transport again (Eq. 1) in steady state.

The rapid weakening of AC might play an important role in the climate system. As one of the strongest western boundary currents, the AC transport a large amount of heat poleward. In a warming climate, the weakening of AC could induce a heat convergence and enhance the warming in the Indian Ocean (Sun et al., 2022; McMonigal et al., 2022). Additionally, changes in the Agulhas Current system in a warming climate might play an important role in modulating the strength of AMOC by changing the salt budget in the Atlantic basin (Beal et al. 2011; Weijer et al. 2003; Biastoch et al. 2009). However, due to the coarse resolution in most of the climate models, the simulated Agulhas Leakage is likely unrealistic, which might affect our understanding how the Agulhas Leakage changes following a weakening of the AC may feed back to the overturning circulation (Weijer et al., 2014). In the future, more state-of-the-art high-resolution climate models are needed to evaluate the potential feedbacks to the Atlantic overturning due to changes in the Agulhas Current and Agulhas leakage.

Acknowledgments

This research is supported by the National Natural Science Foundation of China (42225601, 42076009) and Fundamental Research Funds for the Central Universities (202072001). S. Sun is supported by Florida State University. Z. Chen is partly supported by the Taishan Scholar Funds (tsqn201812022). The authors thank all anonymous reviewers for providing constructive comments.

Open Research

The CESM large ensemble data were downloaded from Climate Data Gateway at NCAR (https://www.earthsystemgrid.org/). The CMIP6 data were downloaded from the Earth System Grid Federation node (https://esgf-node.llnl.gov/search/cmip6/). The reduced gravity model is

401 available at the online open access repository figshare
402 (https://doi.org/10.6084/m9.figshare.12903086) under a "CC BY 4.0" licence. The MITgcm
403 experiments source code and the data used to generate figures are now available in figshare
404 (https://doi.org/10.6084/m9.figshare.21802770).
405
406 **References**

407 Allison, L. C., H. L. Johnson, and D. P. Marshall (2011). Spin-up and adjustment of the
408 Antarctic Circumpolar Current and global pycnocline. *Journal of Marine*
409 *Research*, 69, 167-189.
410 Beal, L. M., S. Elipot, A. Houk, and G. M. Leber (2015). Capturing the Transport
411 Variability of a Western Boundary Jet: Results from the Agulhas Current Time-
412 Series Experiment (ACT). *Journal of Physical Oceanography*, 45, 1302-1324.
413 Beal, L. M., W. P. De Ruijter, A. Biastoch, R. Zahn, and S. W. I. W. Group (2011). On
414 the role of the Agulhas system in ocean circulation and climate. *Nature*, 472,
415 429-436.
416 Beal, L. M., and S. Elipot (2016). Broadening not strengthening of the Agulhas Current
417 since the early 1990s. *Nature*, 540, 570-573.
418 Bellomo, K., Angeloni, M., Corti, S., & von Hardenberg, J. (2021). Future climate
419 change shaped by inter-model differences in Atlantic meridional overturning
420 circulation response. *Nature Communications*, 12, 3659.
421 Biastoch, A., C. W. Böning, and J. Lutjeharms (2008a). Agulhas leakage dynamics
422 affects decadal variability in Atlantic overturning circulation. *Nature*, 456, 489-
423 492.
424 Biastoch, A., J. R. E. Lutjeharms, C. W. Böning, and M. Scheinert (2008b). Mesoscale
425 perturbations control inter-ocean exchange south of Africa. *Geophysical*
426 *Research Letters*, 35.
427 Biastoch, A., C. W. Boning, F. U. Schwarzkopf, and J. R. Lutjeharms (2009). Increase
428 in Agulhas leakage due to poleward shift of Southern Hemisphere westerlies.
429 *Nature*, 462, 495-498.

Bonan, D. B., A. F. Thompson, E. R. Newsom, S. Sun, and M. Rugenstein (2022) Transient and equilibrium responses of the Atlantic overturning circulation to warming in coupled climate models: the role of temperature and salinity. *Journal of Climate*, 1-42.

Bryden, H. L., L. M. Beal, and L. M. Duncan (2005). Structure and Transport of the Agulhas Current and Its Temporal Variability. *Journal of Oceanography*, 61, 479-492.

Capotondi, A., M. A. Alexander, N. A. Bond, E. N. Curchitser, and J. D. Scott (2012). Enhanced upper ocean stratification with climate change in the CMIP3 models. *Journal of Geophysical Research: Oceans*, 117.

Chen, C., G. Wang, S.-P. Xie, and W. Liu (2019). Why Does Global Warming Weaken the Gulf Stream but Intensify the Kuroshio? *Journal of Climate*, 32, 7437-7451.

Chen, G., J. Lu, and D. M. W. Frierson (2008). Phase Speed Spectra and the Latitude of Surface Westerlies: Interannual Variability and Global Warming Trend. *Journal of Climate*, 21, 5942-5959.

Chen, Z., L. Wu, B. Qiu, S. Sun, and F. Jia (2014). Seasonal Variation of the South Equatorial Current Bifurcation off Madagascar. *Journal of Physical Oceanography*, 44, 618-631.

Cheng, W., J. C. H. Chiang, and D. Zhang (2013). Atlantic Meridional Overturning Circulation (AMOC) in CMIP5 Models: RCP and Historical Simulations. *Journal of Climate*, 26, 7187-7197.

Eyring, V., S. Bony, G. A. Meehl, C. A. Senior, B. Stevens, R. J. Stouffer, and K. E. Taylor (2016). Overview of the Coupled Model Intercomparison Project Phase 6 (CMIP6) experimental design and organization. *Geoscientific Model Development*, 9, 1937-1958.

Feng, M., X. Zhang, B. Sloyan, and M. Chamberlain (2017). Contribution of the deep ocean to the centennial changes of the Indonesian Throughflow. *Geophysical Research Letters*, 44, 2859-2867.

Godfrey, J. S. (1989). A sverdrup model of the depth-integrated flow for the world ocean allowing for island circulations. *Geophysical & Astrophysical Fluid Dynamics*, 45, 89-112.

460 Goyal, R., A. Sen Gupta, M. Jucker, and M. H. England (2021). Historical and
461 Projected Changes in the Southern Hemisphere Surface Westerlies. *Geophysical*
462 *Research Letters*, 48, e2020GL090849.
463 Gent, P. R., and J. C. Mcwilliams (1990). Isopycnal mixing in ocean circulation models,
464 *Journal of Physical Oceanography*, 20(1), 150–155.
465 Gunn, K. L., L. M. Beal, S. Elipot, K. McMonigal, and A. Houk (2020). Mixing of
466 Subtropical, Central, and Intermediate Waters Driven by Shifting and Pulsing of
467 the Agulhas Current. *Journal of Physical Oceanography*, 50, 3545-3560.
468 Hu, S., J. Sprintall, C. Guan, M. J. McPhaden, F. Wang, D. Hu, and W. Cai (2020)
469 Deep-reaching acceleration of global mean ocean circulation over the past two
470 decades. *Science Advances*, 6, eaax7727.
471 Huang, R. X., M. A. Cane, N. Naik, and P. Goodman (2000). Global adjustment of the
472 thermocline in response to deepwater formation. *Geophysical Research Letters*,
473 27, 759-762.
474 Johnson, H. L., and D. P. Marshall (2004). Global Teleconnections of Meridional
475 Overturning Circulation Anomalies. *Journal of Physical Oceanography*, 34,
476 1702-1722.
477 Kay, J. E., and Coauthors (2015). The Community Earth System Model (CESM) Large
478 Ensemble Project: A Community Resource for Studying Climate Change in the
479 Presence of Internal Climate Variability. *Bulletin of the American*
480 *Meteorological Society*, 96, 1333-1349.
481 Li, G., L. Cheng, J. Zhu, K. E. Trenberth, M. E. Mann, and J. P. Abraham (2020).
482 Increasing ocean stratification over the past half-century. *Nature Climate*
483 *Change*, 10, 1116-1123.
484 Ma, J., M. Feng, J. Lan, and D. Hu (2020): Projected Future Changes of Meridional
485 Heat Transport and Heat Balance of the Indian Ocean. *Geophysical Research*
486 *Letters*, 47.
487 Marshall, J., A. Adcroft, C. Hill, L. Perelman, and C. Heisey (1997). A finite-volume,
488 incompressible Navier Stokes model for studies of the ocean on parallel
489 computers. *Journal of Geophysical Research: Oceans*, 102, 5753-5766.

McMonigal, K., K. L. Gunn, L. M. Beal, S. Elipot, and J. K. Willis (2022). Reduction in Meridional Heat Export Contributes to Recent Indian Ocean Warming. *Journal of Physical Oceanography*, 52, 329-345.

McMonigal, K., L. M. Beal, S. Elipot, K. L. Gunn, J. Hermes, T. Morris, and A. Houk (2020). The Impact of Meanders, Deepening and Broadening, and Seasonality on Agulhas Current Temperature Variability. *Journal of Physical Oceanography*, 50, 3529-3544.

Peng, Q., and Coauthors (2022). Surface warming-induced global acceleration of upper ocean currents. *Science Advances*, 8, eabj8394.

Rühs, S., J. V. Durgadoo, E. Behrens, and A. Biastoch (2013). Advective timescales and pathways of Agulhas leakage. *Geophysical Research Letters*, 40, 3997-4000.

Sen Gupta, A., S. McGregor, E. van Sebille, A. Ganachaud, J. N. Brown, and A. Santoso (2016) Future changes to the Indonesian Throughflow and Pacific circulation: The differing role of wind and deep circulation changes. *Geophysical Research Letters*, 43, 1669-1678.

Sen Gupta, A., A. Stellema, G. M. Pontes, A. S. Taschetto, A. Vergés, and V. Rossi (2021). Future changes to the upper ocean Western Boundary Currents across two generations of climate models. *Scientific Reports*, 11, 9538.

Stellema, A., A. Sen Gupta, and A. S. Taschetto (2019). Projected slow down of South Indian Ocean circulation. *Scientific Reports*, 9, 17705.

Sun, S., and A. F. Thompson (2020) Centennial Changes in the Indonesian Throughflow Connected to the Atlantic Meridional Overturning Circulation: The Ocean's Transient Conveyor Belt. *Geophysical Research Letters*, 47.

Sun, S., L. Wu, and B. Qiu (2013). Response of the Inertial Recirculation to Intensified Stratification in a Two-Layer Quasigeostrophic Ocean Circulation Model. *Journal of Physical Oceanography*, 43, 1254-1269.

Sun, S., A. F. Thompson, and I. Eisenman (2020). Transient Overturning Compensation between Atlantic and Indo-Pacific Basins. *Journal of Physical Oceanography*, 50, 2151-2172.

519 Sun, S., A. F. Thompson, S.-P. Xie, and S.-M. Long (2022). Indo-Pacific Warming
520 Induced by a Weakening of the Atlantic Meridional Overturning Circulation.
521 *Journal of Climate*, 35, 815-832.
522 Talley, D. L. (2013). Closure of the Global Overturning Circulation Through the Indian,
523 Pacific, and Southern Oceans: Schematics and Transports. *Oceanography*, 26.
524 Wang, Y., F. J. Beron-Vera, and M. J. Olascoaga (2016). The life cycle of a coherent
525 Lagrangian Agulhas ring. *Journal of Geophysical Research: Oceans*, 121, 3944-
526 3954.
527 Weijer, W., W. P. M. De Ruijter, A. Sterl, and S. S. Drijfhout (2002). Response of the
528 Atlantic overturning circulation to South Atlantic sources of buoyancy. *Global*
529 *and Planetary Change*, 34, 293-311.
530 Weijer, W., & van Sebille, E. (2014). Impact of Agulhas Leakage on the Atlantic
531 Overturning Circulation in the CCSM4, *Journal of Climate*, 27(1), 101-110.
532 Weijer, W., W. Cheng, O. A. Garuba, A. Hu, and B. T. Nadiga (2020). CMIP6 Models
533 Predict Significant 21st Century Decline of the Atlantic Meridional Overturning
534 Circulation. *Geophysical Research Letters*, 47, e2019GL086075.
535 Yang, H., and Coauthors (2020). Poleward Shift of the Major Ocean Gyres Detected in
536 a Warming Climate. *Geophysical Research Letters*, 47, e2019GL085868.
537 Zhang, R., S. Sun, Z. Chen, H. Yang and L. Wu (2023). On the decadal and multi-decadal
538 variability of the Agulhas Current, *Journal of Physical Oceanography,*
539 https://doi.org/10.1175/JPO-D-22-0123.1
540 Zhang, X., Q. Wang, and M. Mu (2017). The impact of global warming on Kuroshio
541 Extension and its southern recirculation using CMIP5 experiments with a high-
542 resolution climate model MIROC4h. *Theoretical and Applied Climatology*, 127,
543 815-827.
544
545
546
547

Geophysical Research Letters

Supporting Information for

Rapid 21st century weakening of the Agulhas Current in a warming climate

Ruize Zhang[1,2,3], Shantong Sun[*4], Zhaohui Chen[*1,2], Haiyuan Yang[1,2] and Lixin Wu[1,2]

1. Frontier Science Center for Deep Ocean Multispheres and Earth System (FDOMES) and Physical Oceanography Laboratory, Ocean University of China, Qingdao, China

2. Laoshan Laboratory, Qingdao, China

3. Academy of the Future Ocean, Ocean University of China, Qingdao, China

4. Department of Earth, Ocean & Atmospheric Science, Florida State University, Tallahassee, US

Contents of this file

Introduction

This supporting information includes three sections of text and fourteen figures. In Text S1, we describe the role of diapycnal mixing. In Text S2, we describe the 1.5-layer reduced gravity model. In Text S3, we describe the configuration for the MITgcm experiments.

Text S1. Role of diapycnal mixing in the Indian Ocean:

The deep overturning circulation in the Indian Ocean might also contribute to the volume transport of AC, but it is small compared to the upper-layer volume transport. In CESM-LENS, the time mean value of the meridional volume transport below 2000 m depth across 32.5 ˚S in the Indian Ocean is 1.43 Sv. This time-mean meridional volume transport is balanced by a weak diapycnal upwelling across 2000 m depth in the Indian Ocean. This is

consistent with the observed low diapycnal diffusivity in the intermediate depth (e.g., LedWell et al., 1993). This is also consistent with modern observations, in which the abyssal overturning circulation is mainly confined to depths below 2000 m depth due to constraints by the bottom topography (Ferrari et al., 2016; de Lavergne et al., 2017).

In the reduced gravity model, the contribution due to the deep overturning is represented as an interior diapycnal upwelling, $w = \kappa/h$, as in previous studies (e.g., Thompson et al., 2016), where κ is 2.0×10^{-5} m^2/s, similar to observations (Waterhouse et al., 2014). This contributes about 1 Sv to the upper ocean transport, consistent with CESM.

Text S2. Description of the 1.5-layer reduced gravity model

The momentum equation of the 1.5-layer reduced gravity model is given by

$$\frac{\partial \vec{u}}{\partial t} + (f + \xi) \times \vec{u} = -\nabla(g'h + \frac{1}{2}|\vec{u}|^2) + A_h\nabla^2\vec{u} + \frac{\vec{\tau}}{\rho_0 h} \quad \text{(S1)}$$

where $\vec{u}$ = (u, v) is the horizontal velocity vector, $\vec{k}$ is the unit vector in the vertical direction, f is the latitude-dependent Coriolis parameter, ζ is relative vorticity, g' = 0.02 m s^{-2} is the reduced gravity, A_h = 1×10^4 m^2 s^{-1} is horizontal viscosity, $\vec{\tau}$ represents surface wind stress, ρ_0= 1035 kg m^{-3} is the reference density, and h is the interface depth as a function of space and time.

The volume conservation equation is given by

$$\frac{\partial h}{\partial t} + \nabla \cdot (h\vec{u}) = \nabla \cdot (K_{GM}\nabla h) + w_{diap} + w_{relax} + w_{NADW}, \quad \textit{(S2)}$$

where K_{GM} = 1000 m^{2}s^{-1} is the eddy thickness diffusivity that represents unresolved mesoscale eddies; w_{diap} is the interior diapycnal velocity parameterized as,

$$w_{diap} = \frac{\kappa}{h} \quad \text{(S3)}$$

with κ = 2.0 × 10^{-5}m^2 s^{-1}; w_{NADW} is a constant velocity specified over the northernmost 5-degree latitude in the North Atlantic and represents NADW formation; and w_{relax} is a simplified representation of water mass transformation in the Southern Ocean, which is expressed as a relaxation to a constant interface depth of h_c = 10 m,

$$W_{\text{relax}} = \lambda\,(h_c - h). \quad \text{(S4)}$$

The relaxation is implemented in the southernmost 10 degrees of latitude with the relaxation timescale λ^{-1} increasing northward linearly from 10 days at the southern boundary (72 ˚S) to 100 days at 62 ˚S. This relaxation in the Southern Ocean essentially fixes the outcropping latitude of the interface. A fast relaxation with λ^{-1} = 1 hr is also included wherever the interface depth is less than h_c in order to avoid negative upper layer thickness. The model is integrated forward using the 3rd order Adams-Bashforth method.

The reduced gravity model is forced by the AMOC strength and wind stress that are derived from CESM-LENS. We calculate the AMOC strength as the maximum value of the AMOC streamfunction at 40 ˚N from 2006 to 2100 in the CESM-LENS. To represent changes in surface wind forcing in a warming climate, we use the zonal component of surface wind stress in CESM-LENS from 2006 to 2100. We also took a zonal average of the wind

stress in each basin. At around 30˚S, the zonal integration of the wind-stress curl in the Indo-Pacific is similar between the reduced gravity model and CESM.

$$taux_{Ind}(y,t) = \frac{\int_{Ind} Taux(x,y,t)dx}{\int_{Ind} dx}, \qquad \text{(S5)}$$

$$taux_{Pac}(y,t) = \frac{\int_{PAC} Taux(x,y,t)dx}{\int_{PAC} dx}, \qquad \text{(S6)}$$

$$taux_{Atl}(y,t) = \frac{\int_{Atl} Taux(x,y,t)dx}{\int_{Atl} dx}, \qquad \text{(S7)}$$

Then we calculate the linear trend at each latitude in each of the basin during 2006 and 2100.

In the control run, we use the wind stress at year 2006 (Figure S2a) and prescribe the NADW formation rate as the AMOC strength at 2006 in the CESM-LENS. We run the model for 4000 years to reach an approximate stable state. Using the control run as initial conditions, we conduct another four experiments as described in the main text. The transport of the Agulhas Current is integrated across the western boundary of Indian Ocean along 32.5 ˚S, $\int_{x_w}^{x_w+\delta x} (vh - K_{GM}\frac{\partial h}{\partial y})\, dx$, where v is the meridional velocity, h is the depth of the upper layer in the reduced gravity model, x_w is the western boundary, and δx is the AC width. More information about the reduced gravity model could be found in Sun et al. (2020).

Text S3. Description of the MITgcm ocean-only experiments

To resolve the depth structure of the Agulhas Current, we also conduct a series of experiments using MITgcm (Marshall et al., 1997). The model domain, discretized on a 1˚ resolution grid, is similar to the reduced gravity model. There are three idealized basins that represent the Atlantic, Indian, and Pacific Ocean, connected in the south by a reentrant channel that represents the Southern Ocean. In the vertical, there are 30 vertical layers ranging from 20 m at the top to 250 m at the bottom. A vertical diffusivity is implemented that is a function of depth and increases from 2.0×10^{-5} m^2 s^{-1} at the surface to 1.0×10^{-4} m^{2}s^{-1} with a transition depth of 2000 m. Vertical convection is represented by an implicit diffusion with a diffusivity of 10 m^2 s^{-1}, whenever the stratification is hydrostatically unstable. Unresolved eddies are represented using the skew-flux form of the Gent-McWilliams (GM) parameterization with an eddy thickness diffusivity K_{GM} = 500 m^2 s^{-1}. Isopycnal diffusion due to eddies are represented using the Redi scheme with K_{Redi} = 500 m^2 s^{-1}. The momentum is dissipated via Laplacian viscosity, biharmonic viscosity, and vertical viscosity with coefficients A_h = 1.0×10^4 m^2 s^{-1}, A_4 = 1.0×10^{12} m^4 s^{-1}, and A_v = 1.0×10^{-3}m^2 s^{-1}, respectively. The biharmonic viscosity is used to suppress grid-scale noise. The model is forced with a zonally-uniform zonal wind stress. Temperature at the surface is restored to a prescribed zonally-uniform temperature profile with a relaxation timescale of 20 days. For the salinity surface boundary condition, we use a prescribed freshwater flux, that is uniform in the zonal direction except in the Pacific Ocean, where an extra constant

freshwater flux is added to suppress convection in the high-latitude North Pacific. For more details about the model configuration, readers are referred to Sun et al. (2022).

We run the model for 2,000 years, at which point the model reaches an approximate steady state. We take the steady state simulation as a control simulation and then apply a 3K warming in the high-latitude North Atlantic Ocean to investigate the role of AMOC remote modulation in AC changes. And to investigate the impact of local sea surface warming to the AC, we apply a 3K warming in the whole Indian Ocean.

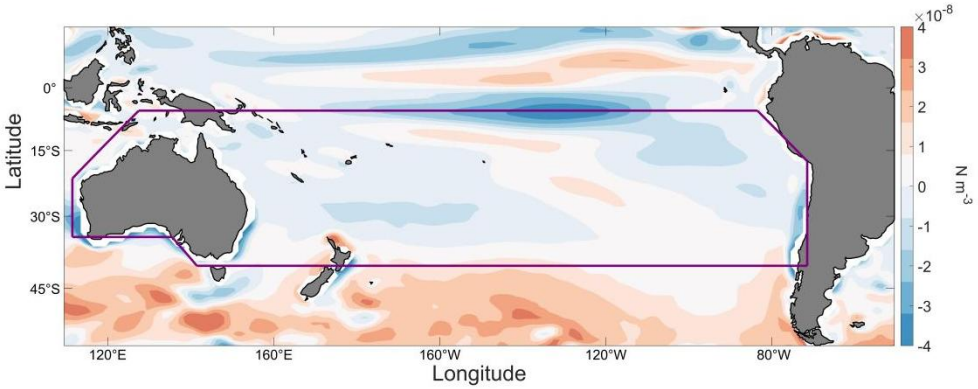

Figure S1 Changes in wind stress curl from 2006 to 2100 in the Pacific Ocean in CESM Large Ensemble. The purple lines denote the integral path for the Island rule (Godfrey 1989). The Island rule is used to estimate the volume transport of ITF, which is integrated by $T_{Island\ Rule} = -\frac{1}{\rho_0 f_s}\oint_c \vec{\tau}\cdot\vec{s}dl$, where the ρ_0 is the reference seawater density, f_s is the Coriolis parameter at the southern boundary of the Pacific Ocean in the integral path and $\vec{\tau}$ is the sea surface wind stress.

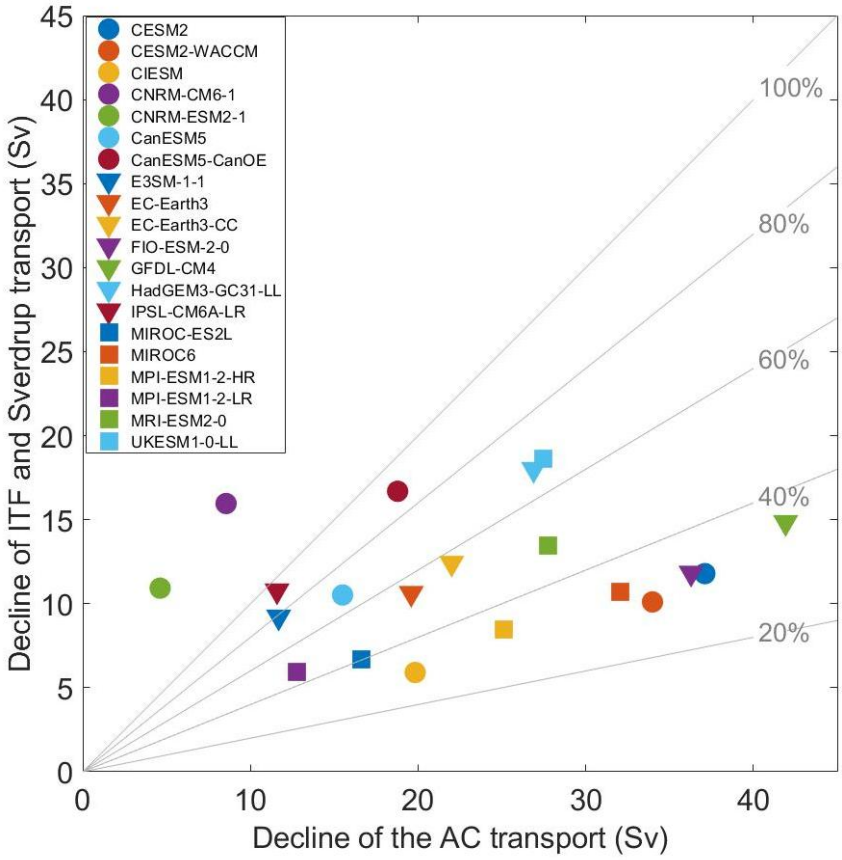

Figure S2. The decline of ITF transport and Sverdrup transport, integrated across the Indian Ocean at 32.5 ˚S, vs the AC volume transport changes from 2015 to 2100 in CMIP6 simulations under the high-end emission scenario ("SSP585"). The gray thin lines are contours in percentage and indicate how much of the AC volume transport reduction can be explained by the decline of the Sverdrup transport and ITF.

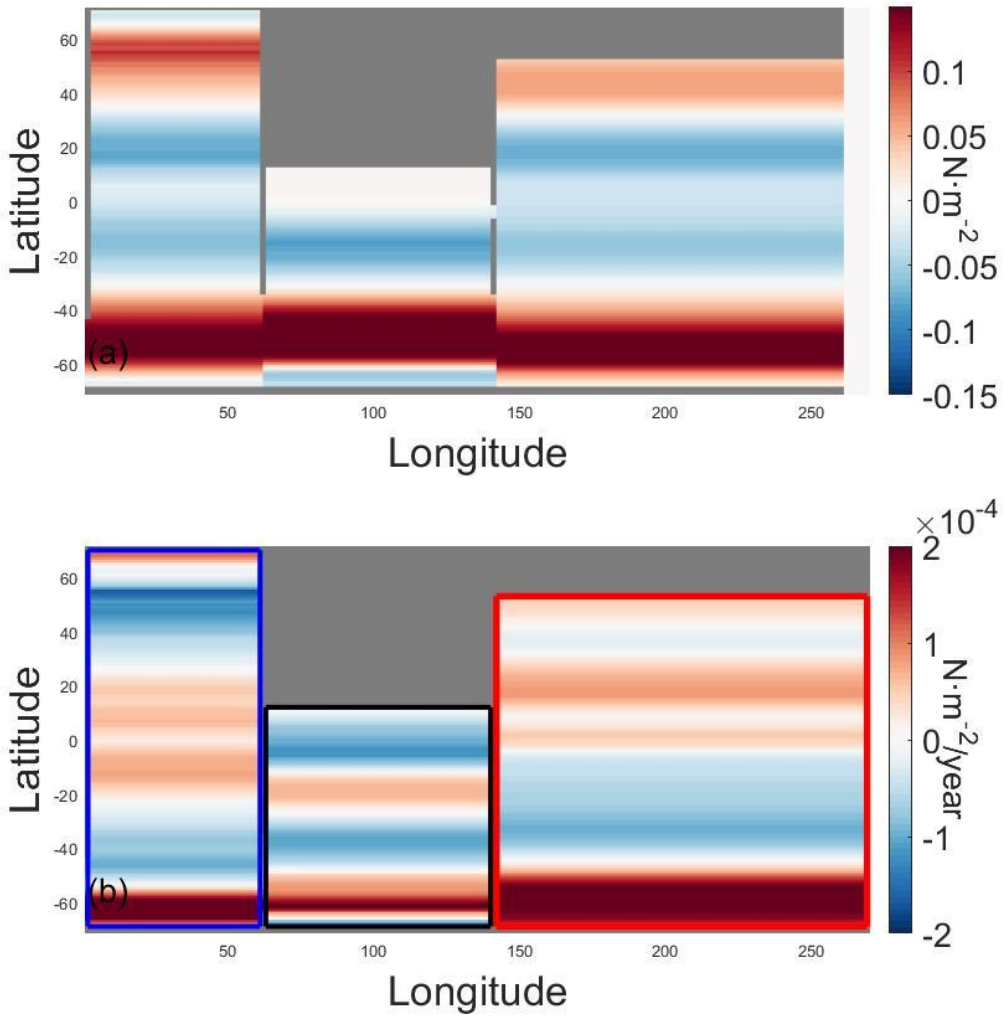

Figure S3. (a) Zonal wind stress used in the 1.5-layer reduced gravity model in the control run and the gray patches represent the lands in the model. (b) The linear trend of the zonal mean wind stress from 2006 to 2100 in three oceans. The blue, black and red contours denote Atlantic Ocean, Indian Ocean and Pacific Ocean, respectively.

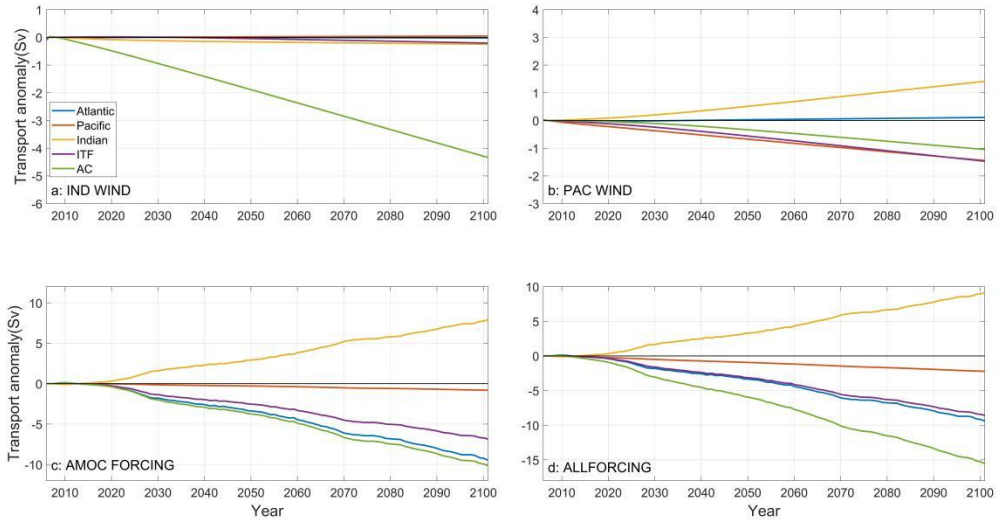

Figure S4. Circulation changes in the reduced gravity model. (a) Changes in the Atlantic meridional volume transport (blue line), Pacific meridional volume transport (orange line), Indian meridional volume transport (yellow line), ITF volume transport and AC volume transport from 2005 to 2100 in IND_WIND experiment. (b) Same as (a) but for the PAC_WIND experiment. (c) Same as (a) but for the AMOC_FORCING experiment. (d) Same as (a) but for the ALLFORCING experiment. Here, positive value in Pacific Ocean, Indian Ocean and Atlantic Ocean denotes northward transport anomaly, while the positive value in ITF and AC denotes eastward transport and southward transport anomaly, respectively.

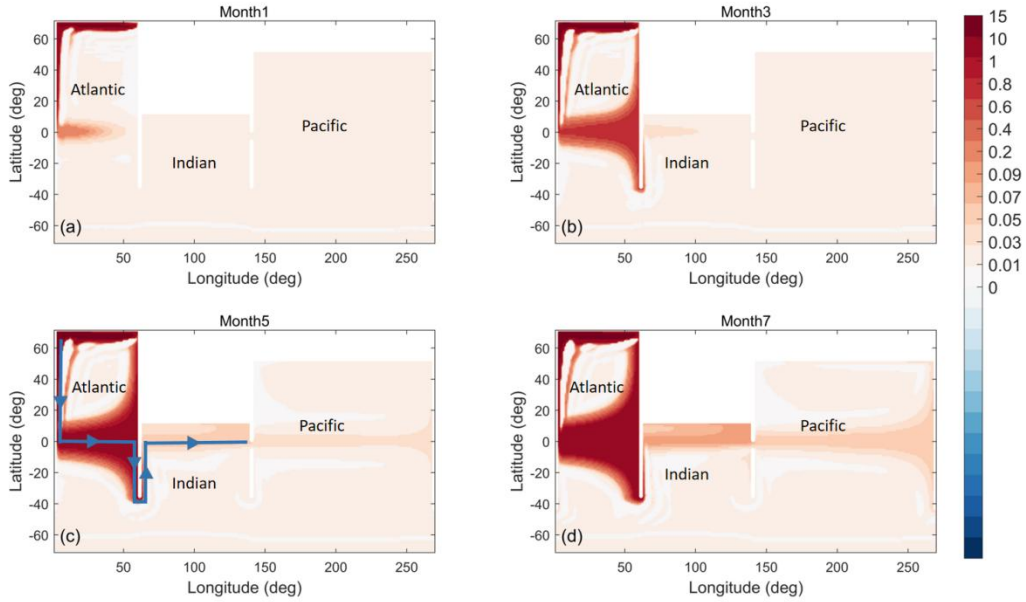

Figure S5. Evolution of interface depth anomaly (m) after an abrupt 6 Sv reduction in NADW formation rate in the reduced gravity model. The four panels show the interface depth anomaly (a) 1 month, (b) 3 months, (c) 5 months, and (d) 7 months after the NADW perturbation. In panel (c), the propagation pathway of Kelvin waves from the North Atlantic into the Indian Ocean is denoted as blue lines with arrows.

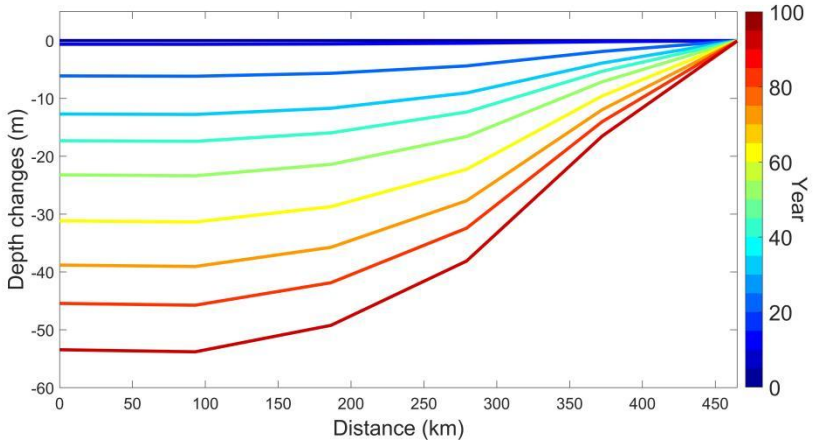

Figure S6. Interface depth changes in the AC section (red line in Figure 1) from 2005 to 2100 in the AMOC_FORCING reduced gravity model experiment. The interface depth anomaly at 450 km is subtracted to highlight changes in the western boundary.

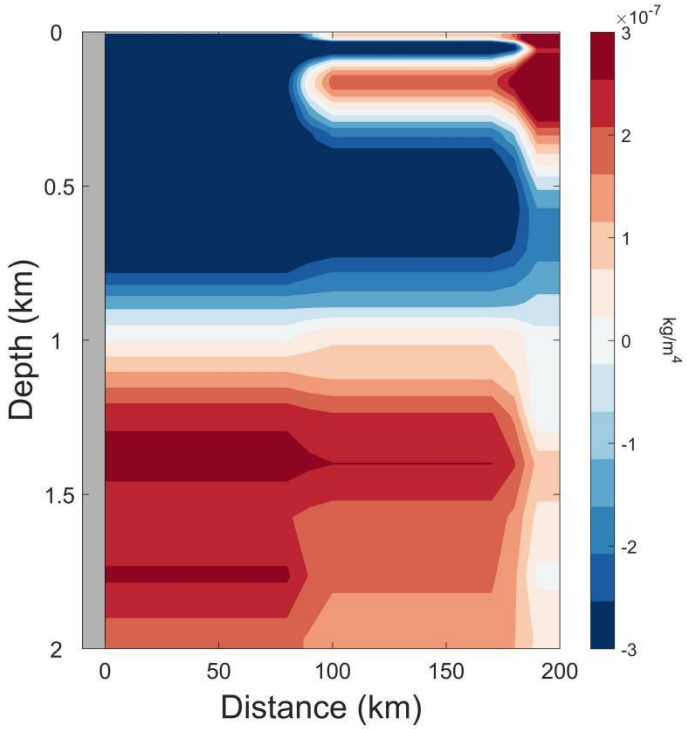

Figure S7. Changes in the offshore in-situ density gradient along the AC section (red line in Figure1) from 2005 to 2100 in the CESM-LENS, calculated as the difference between the value averaged over the first 10 years and the last 10 years.

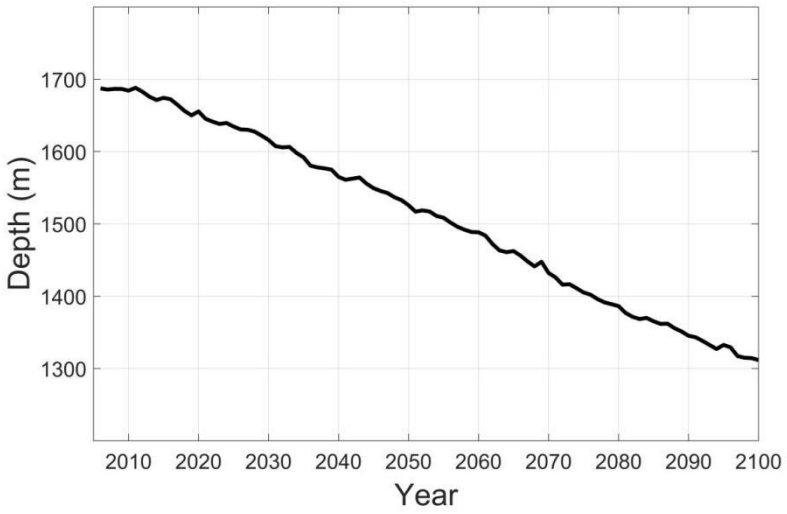

Figure S8. Evolution of the AC depth, defined as the maximum depth of 1 cm/s contour from 2006 to 2100 in CESM-LENS.

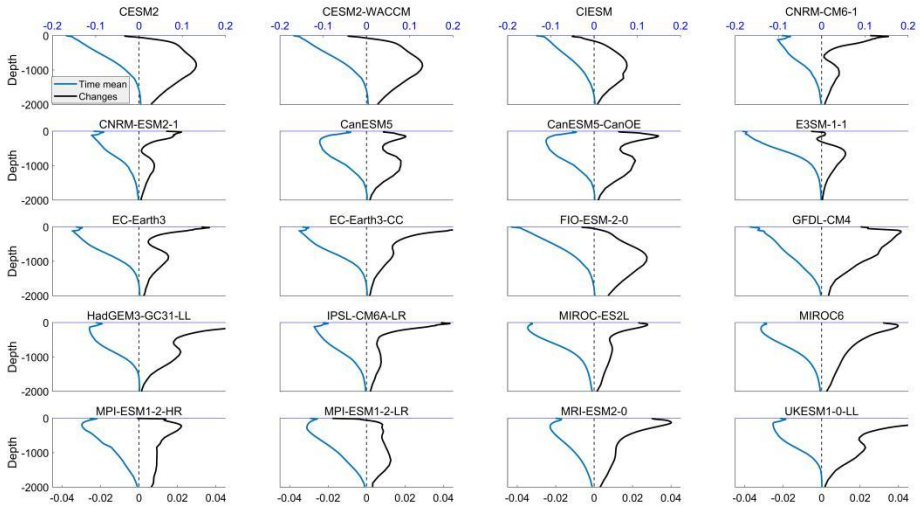

Figure S9. Vertical changes in the horizontal averaged AC velocity from 2015 to 2100 in CMIP6 models under the high-end emission scenario "SSP585" (black line) and the vertical distribution of the horizontal averaged AC velocity (m/s) averaged from 2015 to 2100 in the CMIP6 models under the high-end emission scenario "SSP585".

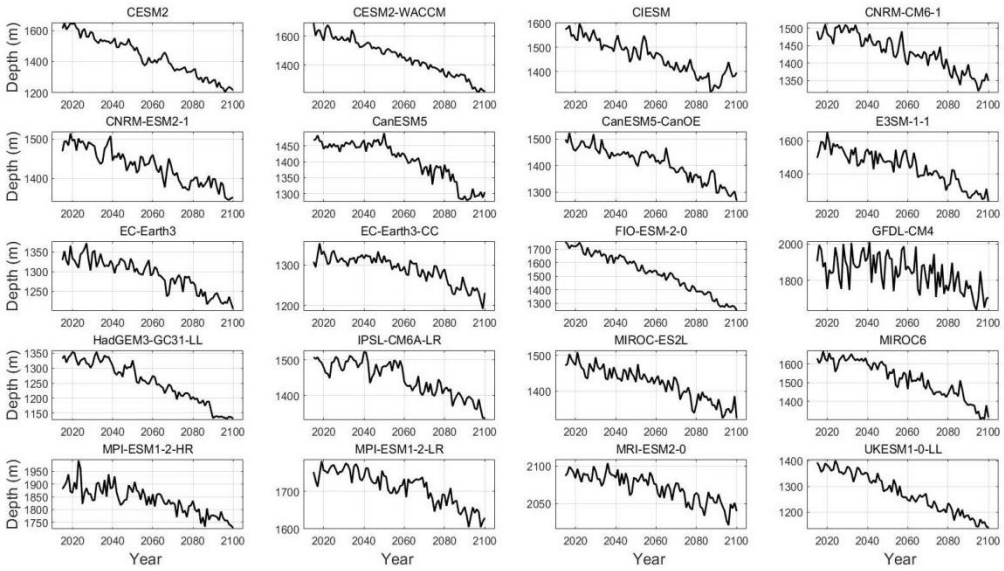

Figure S10. Changes in the AC depth from (m) 2015 to 2100 in CMIP6 models under the high-end emission scenario "SSP585".

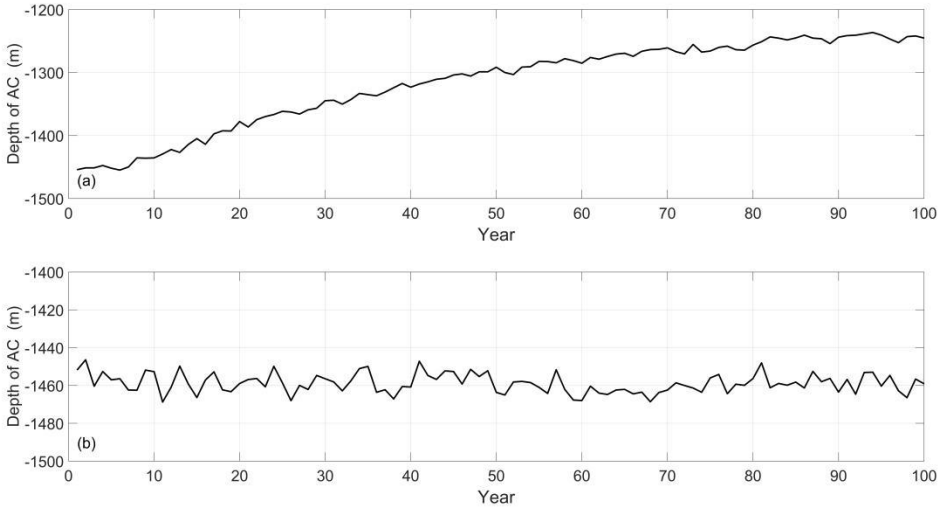

Figure S11. Changes in the AC depth in the (a) "AMOC weakening" experiment, (b) "Indian Ocean warming" experiment, carried out with MITgcm.

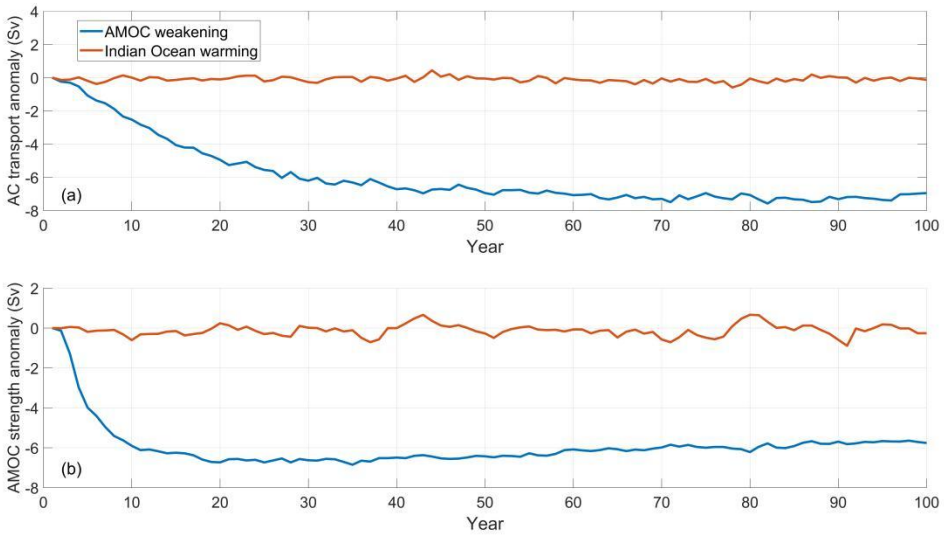

Figure S12. (a) Changes in the AC volume transport anomaly in MITgcm: "AMOC weakening" experiment (blue line), "Indian Ocean warming" experiment (orange line). (b) Same as (a) but for the AMOC strength anomaly.

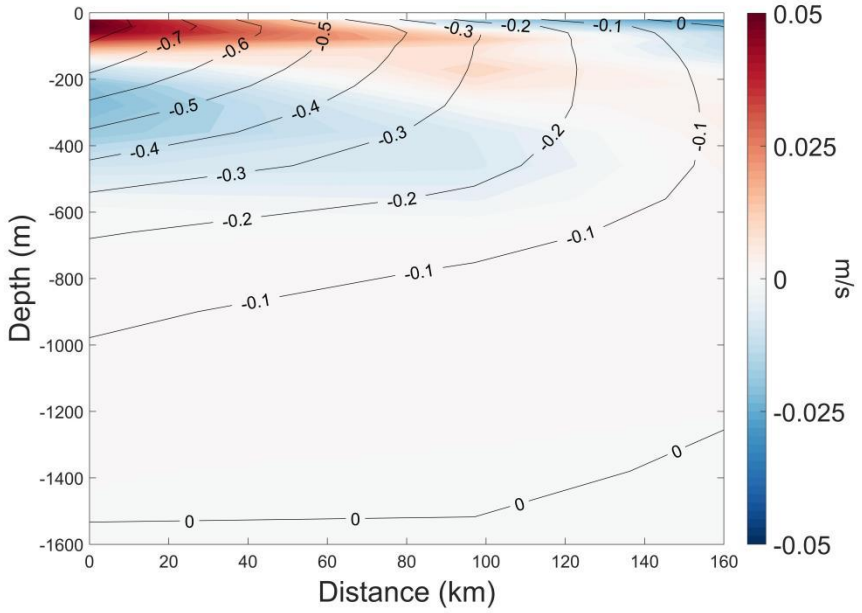

Figure S13. Velocity changes (m/s) in the AC section in the "Indian Ocean warming" experiment. The black contours denote the time-mean velocity of AC.

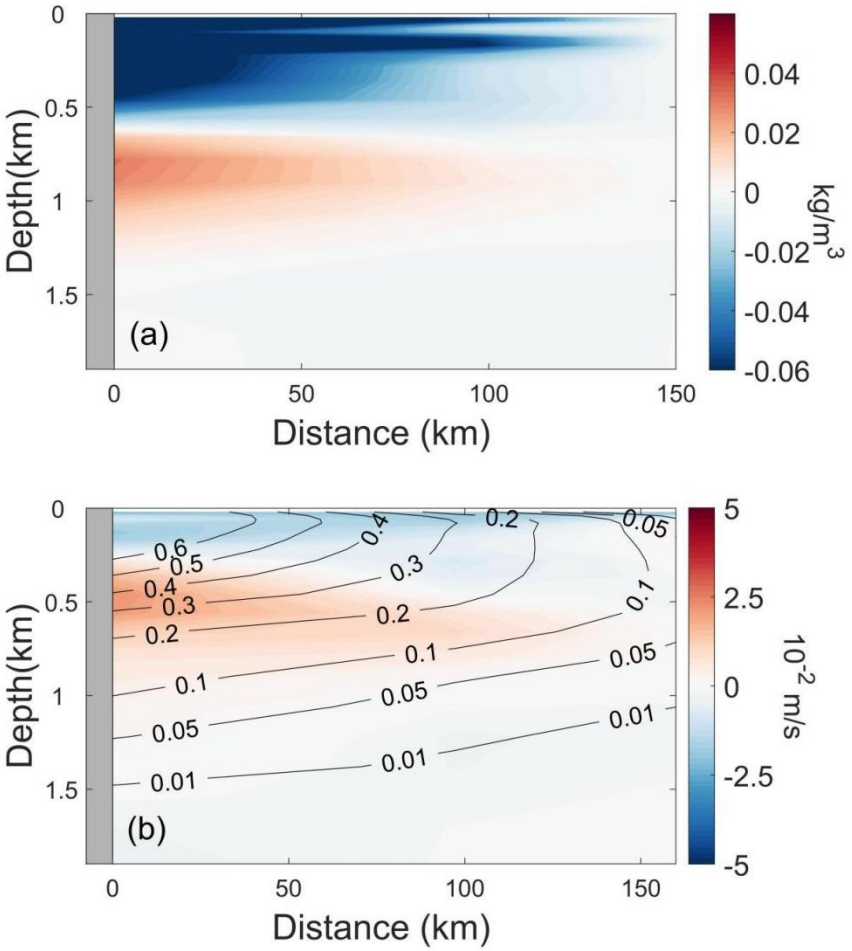

Figure S14. Results in the "Strengthening Westerlies" MITgcm experiment, in which the Southern hemisphere westerlies is strengthened by 10%. (a) Changes in the in-situ density (kg/m3) along the AC cross-section in the "Strengthening Westerlies" experiment. The density anomaly on the right boundary (x=160 km is subtracted to highlight the offshore density gradient. (b) Velocity changes (m/s) in the AC section in the "Strengthening Westerlies" experiment. The black contours denote the time-mean velocity of AC. The gray patch in the left side denotes the coast of Africa.

References

de Lavergne, C., Madec, G., Roquet, F. et al. (2017) Abyssal ocean overturning shaped by seafloor distribution. *Nature* 551, 181-186.

760 Ferrari R., Mashayek A., McDougall T. J., Nikurashin M., Campin J.-M. (2016).
761 Turning ocean mixing upside down. *Journal of Physical Oceanography* 46 (7),
762 2239-2261.
763 Godfrey, J. S., (1989) A sverdrup model of the depth-integrated flow for the world
764 ocean allowing for island circulations. *Geophysical & Astrophysical Fluid*
765 *Dynamics*, **45**, 89-112.
766 Ledwell, J., Watson, A. & Law, C. (1993) Evidence for slow mixing across the
767 pycnocline from an open-ocean tracer-release experiment. *Nature* 364, 701-703.
768 Marshall, J., A. Adcroft, C. Hill, L. Perelman, and C. Heisey (1997). A finite-volume,
769 incompressible Navier Stokes model for studies of the ocean on parallel
770 computers. *Journal of Geophysical Research: Oceans*, 102, 5753-5766.
771 Sun, S., A. F. Thompson, and I. Eisenman (2020). Transient Overturning Compensation
772 between Atlantic and Indo-Pacific Basins. *Journal of Physical Oceanography*,
773 50, 2151-2172.
774 Sun, S., A. F. Thompson, S.-P. Xie, and S.-M. Long (2022). Indo-Pacific Warming
775 Induced by a Weakening of the Atlantic Meridional Overturning Circulation.
776 *Journal of Climate*, 35, 815-832.
777 Thompson, A. F., A. L. Stewart, and T. Bischoff (2016) A Multibasin Residual-Mean
778 Model for the Global Overturning Circulation, *Journal of Physical*
779 *Oceanography*, 46(9), 2583–2604.
780 Waterhouse, A., MacKinnon, J. A., Nash, J. D., Alford, M. H., Kunze, E., Simmons, H.
781 L., et al. (2014). Global patterns of diapycnal mixing from measurements of the
782 turbulent dissipation rate. *Journal of Physical Oceanography*, 44(7), 1854-1872.
783
784
785